PERIODICO di MINERALOGIA Volume 91, No. 4, 2022
ISSN: 0369-8963

Performance Analysis of An Intelligent Adaptive Rbfnn Based Novel Mmc-Dstatcom in Grid Connected Pv System

C. UMADEVI[1,*], M. GNANA SUNDARI[2] AND P. SUBHA KARUVELAM[3]

[1]C. Umadevi, Research Scholar, Department of Electrical and Electronics Engineering, Government College of Engineering, Tirunelveli, Tamilnadu

[2]M. Gnana Sundari, Professor, Department of Electrical and Electronics Engineering, Government College of Engineering, Tirunelveli, Tamilnadu.

[3]P. Subha Karuvelam, Professor, Department of Electrical and Electronics Engineering, Government College of Engineering, Tirunelveli, Tamilnadu.

[*]Corresponding author: C. UMADEVI

Abstract

This paper presents a novel Modular Multilevel Converter–DSTATCOM topology used to integrate PV system into the AC Grid. Unlike the conventional MMC topologies, the proposed topology can be applied in high power applications requiring more voltage levels using less capacitor count maintaining higher efficiency. The common problem caused within a MMC by the impact of circulating current is eliminated here by adding it with the input current of each arm. Photovoltaic (PV) System generally uses Power electronic converters to convert the generated DC into AC by switching ON and OFF of the Power electronic devices. This leads to the introduction of Harmonics into the power system causing deterioration in the power quality resulting conductors heating, malfunctioning of fuses, circuit breakers and relays. This paper introduces an Adaptive Radial Basis Function Neural Network (RBFNN) based on the Synchronous Reference Frame (SRF) theory which is capable of generating the compensating reference current needed to extract the total harmonics from the system. It uses a deep learning filtering algorithm based on a hybrid learning method, which is regarded as the computationally efficient training method with less complexity and negligible training time. Extensive simulations are carried out in MATLAB software and its performance in each aspect is analyzed by comparing it with conventional methods. The results obtained show the usefulness of the novel topology and the proposed algorithm in improving power quality.

Key words: *DSTATCOM; MMC; Adaptive RBFNN; SRF; deep learning filtering algorithm.*

Introduction

Increase in consumption of electrical energy has increased the curiosity in electric power productions through Renewable Energy (RE) sources. The awareness among the population on the environmental impacts of continuous fossil fuel usage is also a major reason to move towards the clean energy resources. Solar Photovoltaic (PV) is regarded as one of the significant low carbon emitting approaches with less manufacturing cost [1-2]. From 2021 to 2025, IEA expects solar to set new global deployment records every year with an average of 125 GW of new capacity annually. The power generated from the PV system is variable with changing environmental conditions. When large scale PV systems are integrated to the grid, it can cause voltage and frequency instability. Hence the standards for integrating the PV system with the grid have to be followed strictly. Maintaining rated amplitude and frequency of near sinusoidal voltage and current in the network as in the grid is called Power Quality (PQ) [19]. Any deterioration in the

 https://doi.org/10.37896/pd91.4/9146

ISSN: 0369-8963

power quality causes a decrease in efficiency of the system and leads to wastage of power.

Integration of PV plants into the AC grid includes power electronic converters for DC to DC conversion and AC to AC conversion, a transformer and power filters. The non-linear operating characteristics of the switching devices used can lead to power quality problems in the utility grid [4]. The converters inject harmonics into the grid due to their low frequency operation to attain desired frequency. Deviation of frequency from the fundamental frequency is a major issue in the PV dominated grid. This Harmonics end up in problems like malfunctioning of fuses or circuit breaker relays and heating of conductors [5].

Seeking efficient methods to track and eliminate the harmonics has become mandatory. Harmonic Extraction falls under three major categories (i) Frequency Domain Technique (ii) Time Domain Technique and (iii) Neural Network methods [2]. The frequency domain techniques depend mainly on the Fourier transformations that transform the distorted current and voltage signals from Time domain to the Frequency domain. Now the fundamental component can be isolated from the harmonics and then the compensating signals can be reconstructed. It can be done in three ways (i) Discrete Fourier Transform (DFT) (ii) Fast Fourier Transform (FFT) and (iii) Recursive Discrete Fourier Transform (RDFT). The main drawback of using frequency domain technique is that it is complex in computation and also it cannot be used in for online extraction. Time Domain Technique in harmonic extraction is of three types (i) Filter Based method (ii) Instantaneous Power Theory and (iii) Synchronous Reference Frame method. Time domain techniques uses filters which are sensitive to noise and can cause oscillations. It may need additional PLL resulting in high cost. To overcome the drawbacks in Time Domain technique and Frequency Domain technique neural network methods involving AI filters are used. It has three major methods (i) Adaptive linear Neuron (ADALINE) (ii) Multilayer Perceptron (MLP) and (iii) RBFNN. Comparing to all other networks RBFNN is found to be more potential as all the other approaches have multiple disadvantageous impacts like extensive Harmonics, complexity, excessive convergence period and lesser reliability [21]-[24]. The Adaptive RBFNN technique based on hybrid learning algorithm is introduced in this study, which effectively involves in approximating the nonlinear operations. Training of data can be done in a sequential manner and it can give better generalization abilities. The optimized result helps in generating more accurate reference current when compared to other conventional methods. This current component is then injected to the power system at PCC through custom power devices used for power quality correction. STATCOM is found to be a potential choice for RE systems to enhance the PQ in traditional systems. The main element of the STATCOM is the Voltage Source Converter (VSC) which is a Modular Multilevel Converter (MMC) in the proposed system. One major merit of using an MMC is that it can possibly interface energy storage system directly with medium or high voltage grid. Some other attractive features of MMC are modular structure, transformer free functioning, easy scalability, less expenditure, fault tolerant capability and easy accessibility [6]-[12]. This topology has typical DC to three phase configuration provided the problems of circulating current within converter arms are taken care of.

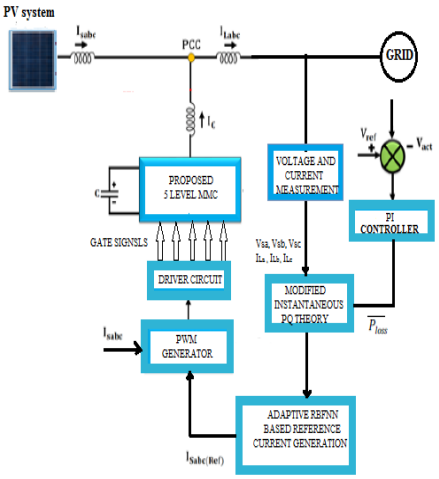

Figure 1. Block diagram of proposed system

Modeling of Solar Photovoltaic Array:

Cells are the basic structure of PV system. Group of cells are joined to form the panels/modules and group of panels make the array

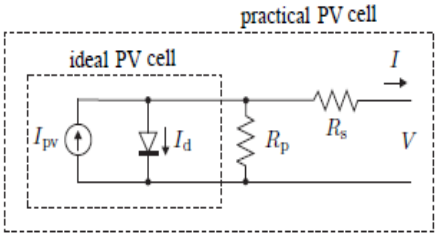

Figure 2. Equivalent circuit of PV cell

From the theory of semiconductor current, equation of ideal PV cell can be derived as

https://doi.org/10.37896/pd91.4/9146

ISSN: 0369-8963

$$I_d = I_{0cell}\left[\exp\left(\frac{qv}{\alpha KT}\right) - 1\right] \quad (1)$$

Where I_d is the diode current

From Figure 1

$$I = I_{PVcell} - I_d \quad (2)$$

$$I = I_{PVcell} - I_{0cell}\left[\exp\left(\frac{qv}{\alpha KT}\right) - 1\right] \quad (3)$$

Practically diode current can also be expressed as

$$I_d = I_0\left(e^{\frac{v_0}{\alpha v_T}} - 1\right) \quad (4)$$

Where α is the ideality constant. For a practical PV cell with series and parallel resistances

$$I = I_{PVcell} - I_{0cell}\left[\exp\left(\frac{v+IR_s}{\alpha v_T}\right) - 1\right] - \frac{V+IR_S}{R_p} \quad (5)$$

The above equation is for a single diode model. There are also other sophisticated methods with 2 diodes or 3 diodes. Photovoltaic datasheets provides PV features, in which Voc n and Isc n represent the nominal open circuit voltage and short circuit current whereas Imp and Vmp signify current and voltage at maximum power point. In addition, Ki and Kv specify the coefficients of Short circuit current / temperature and open circuit voltage/temperature whereas Pmax e represents the maximum experimental peak output power.

R_s is the sum of several structure resistances and R_p exists due to leakage current depends on the fabrication process. In practical PV system R_p is high and R_s is less. The I-V curve depends on internal characteristics (R_s , R_p) and external influence like irradiation and temperature

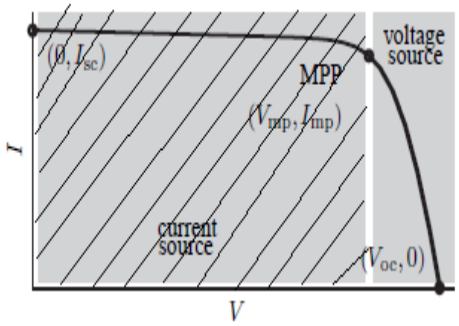

Figure 3. V-I characteristics of PV cell

Light generated PV current I_{pv} relies on the influence of irradiation level and temperature. The equation is

$$Ipv = (Ipv\ n + K_i\Delta_T)\frac{G}{G_n} \quad (6)$$

Where, the produced current at nominal state id signified as Ipv n, the difference among actual and nominal temperatures is signified as Δ_T, irradiation on surface of device is signified as G and nominal irradiance is signified as Gn.

Diode saturation current based on temperature

$$I_0 = I_0n\left(\frac{T_n}{T}\right)^3 \exp\left[\frac{qE_g}{\alpha K}\left(\frac{1}{T_n} - \frac{1}{T}\right)\right] \quad (7)$$

Band Gap energy Eg ≈ 1.2ev (for Si at 25°c) from the diode equation,

$$I_0n = \frac{Isc\ n}{\exp\left(\frac{Voc\ n}{\alpha Vtn}\right)-1} \quad (8)$$

Nominal saturation current I_0n can be indirectly attained through equation (8).The ideality factor α can be ranging from 1≤ α ≤ 1.5. The photovoltaic model can be improved by modifying the equation as

$$I_0 = \frac{Isc\ n + k_i\Delta_T}{\exp\left(\frac{Voc\ n + K_v\Delta_T}{\alpha V_{tn}}\right)-1} \quad (9)$$

The value of band gap energy E_g for T= Tmax can be found from equation (7) as

$$Eg = -\ln\left(\frac{\frac{Isc\ Tmax}{I_0}\left(\frac{T_n}{T_{max}}\right)^3}{\exp\left(\frac{q\ Voc\ Tmax}{\alpha N_S KT_{max}}\right)-1}\right)\frac{\alpha KT_nT_{max}}{q(T_n - T_{max})} \quad (10)$$

Here $V_t = \frac{N_sk_T}{q}$; $I_{sc}\ T_{max} = Isc\ n + K_i\ \Delta I$; $Voc\ T_{max} = Voc\ n + K_v\Delta_T$; $\Delta_T = T_{max} - T_n$.

The only values remaining unknown are the series and parallel resistances R_s and R_p which can be determined by comparing $Pmax\ m = Pmax\ e$; Pmax m is the maximum experimental power given in the datasheet and Pmax e is the maximum experimental power at the maximum power point.

$$Pmax\ m = Pmax\ e = V_{mp}\left[I_{pv} - I_0\left(\exp\frac{q}{KT}\frac{Vmp + R_sImp}{\alpha N_s} - 1\right) - \frac{Vmp + R_sImp}{R_p}\right] \quad (11)$$

$$R_p = \frac{Vmp(Vmp + R_sImp)}{VmpIpv - VmpI_0\exp\left(\frac{q\ (Vmp + R_sImp)}{\alpha N_S KT}\right) + VmpI_0 - Pmax\ e} \quad (12)$$

The value of R_s and R_p can also be found from the iterative method. The aim is to determine the R_s value from which the value of R_p can be found. The iterations are done until

Pmax m = Pmax e

Iterative method helps to improve the model. Every iteration updates the R_s and R_p towards the optimal solution

$$Ipv\ n = \frac{R_s + R_p}{R_p} Isc\ n \quad (13)$$

The above equation gives the light generated current Ipv. R_s and R_p are initially unknown. Initial guess of R_s and R_p are necessary before the iteration. Initial value of R_s is Zero and R_p can be found by

$$R_{p\ min} = \frac{Vmp}{Iscn - Imp} - \frac{Voc\ n - Vmp}{Imp} \quad (14)$$

The above equation gives a good initial guess of R_p

Maximum Power Point Tracking (MPPT)

For extracting the maximum power from Photovoltaic array, global MPPT algorithm is

https://doi.org/10.37896/pd91.4/9146

ISSN: 0369-8963

employed. All the panels are assumed to operate at a same temperature and irradiation. Therefore only current and voltage from one sub module can be considered. Initially the PV voltage is set to open circuit voltage and the current at Voc is zero. A small change in voltage (ΔVpv) is made. The power at K^{th} instant is given as

$$Ppv = Vpv(k)Ipv(k) \quad (15)$$

ΔPpv(k) and ΔVpv(k) are calculated and $\frac{\Delta Ppv}{\Delta Vpv}$ can be determined. The PV panel reaches to maximum power point if $\left|\frac{\Delta Ppv}{\Delta Vpv}\right| \leq \varepsilon$. where ε is a very small number.

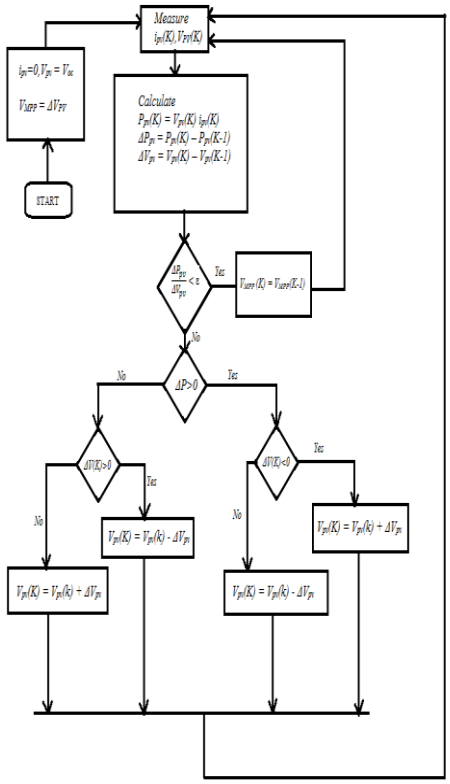

Figure 4. Flow chart of MPPT algorithm

Modelling of 5 level MMC Topology:

Modular Multilevel Converters are the subfamily of multilevel converters. Multicell converters are known for its high degree of modularity, lowest expense for redundancy, lowest harmonic content with large number of output levels, Simple structure and less manufacturing cost. Modular Multilevel converter being a Multicell converter has attracted the attention of industries that are being developed as a solution for HVDC transmission. The introduced MMC has a DC to three phase converter configuration and a half bridge power cell topology. The half bridge methodology is used as DC source since it can operate only on positive and zero voltages. An arm inductances 'L' is series linked all groups of cells for limiting the current because of the rapid voltage variations of arms. The complexity and time consumed can be reduced by considering all power cells in all arms as one equivalent voltage source during simulation. The output of the simulation model can be further refined by including the effects of switching and the dynamic behavior of capacitor. For stable operation of MMC, the average capacitor voltage, impact of circulating currents, stress on power cells have to be adjusted and controlled. Many control strategies and sorting algorithms has been proposed in the literatures. However these methods lacked efficiency and requires extreme convergence period. In case of sorting algorithms, the process of selecting ideal position is highly complex. In the proposed method, the capacitor voltage imbalance among the arm can be controlled by distributing energy between the arms by varying current reference. In addition, the voltage imbalance within each arm is regulated by modifying the converter switching pattern.

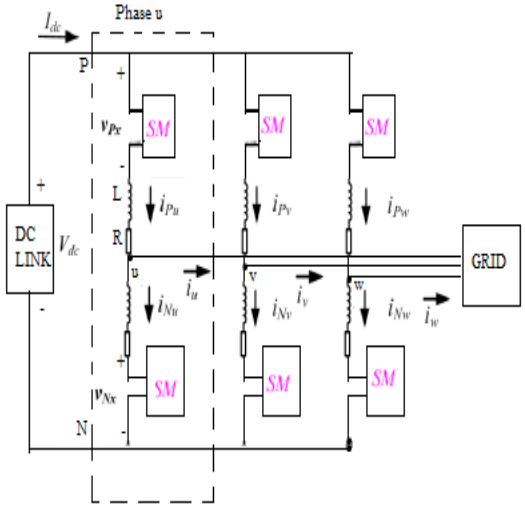

Figure 5. Topology of MMC-DSTATCOM

https://doi.org/10.37896/pd91.4/9146

ISSN: 0369-8963

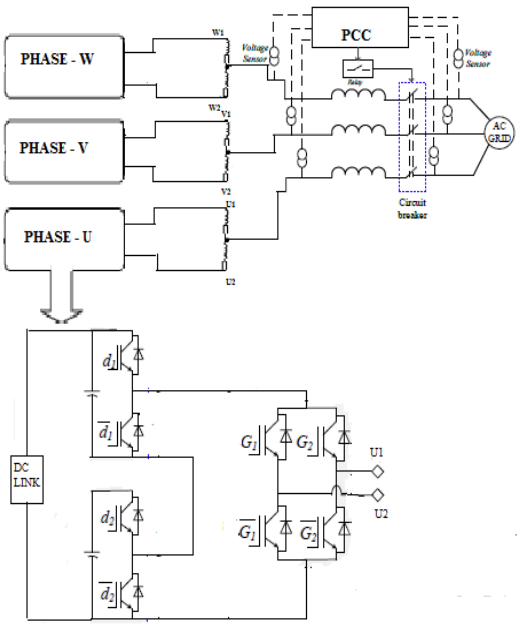

Figure 6. Configuration of MMC- DSTATCOM for grid connected PV system

Figure shows the 5 level three phase MMC topology where each phase leg has two sub modules. Each submodule produces an voltage level of either V_{dc} or 0. Considering two sub modules the sum ranges from 0 to 2 V_{dc}. The sub module in each arm is considered as a voltage source say v_{px}, v_{nx} the upper and lower arm voltages. Similarly Ipx and Inx are the currents in each arm. X refers to the phase v_x is the ac output voltage of phase X. The aim of the MMC is to control the voltages in both the arms and maintain it to be sinusoidal with DC offsets less than half of the DC link voltage with opposite phases.

Considering any phase x

Applying KVL

$$\frac{1}{2}Vdc = v_{px} + L\frac{dipx}{dt} + Ripx + v_x \quad (16)$$

$$\frac{1}{2}Vdc = v_{nx} + \frac{dinx}{dt} + Rinx - v_x \quad (17)$$

Applying KCL

$$i_x = i_{px} - i_{nx} \quad (18)$$

Assume a variable v_{1x}

$$v_{1x} = \frac{1}{2}(v_{px} - v_{nx}) \quad (19)$$

Substituting equation (18) and (19) in (16) and (17) we get

$$\frac{1}{2}L\frac{dix}{dt} + \frac{1}{2}Rix = -v_x - v_{1x} \quad (20)$$

As the low frequency voltage drops are lesser than V_x, the ac voltage (v_x) can be found by v_{1x} when the MMC works as an inverter without current control.

Assume a control variable v_{2x} as

$$v_{2x} = \frac{1}{2}(v_{px} + v_{nx}) \quad (21)$$

The circulating current i_{zx} flows through both arms

$$i_{zx} = (i_{px} + i_{nx}) \quad (22)$$

Substituting equation (21) and (22) in (17) and (18) we get

$$L\frac{di_{zx}}{dt} + Ri_{zx} = \frac{1}{2}Vdc - v_{2x} \quad (23)$$

According to KCL

$$I_d = i_{px} = i_{nx} = \frac{1}{2}(i_{px} + i_{nx}) = i_{zx} \quad (24)$$

The above equations show that the DC link voltage is continuous and the circulating current i_{zx} is regulated by V_{2x}. The DC component of i_{zx} governs the average power at the DC side.

Capacitor voltage balancing in proposed method is done by controlling the energy stored in the capacitor of each arm

$$W_{cpx} = \frac{1}{2}C{v_{cpxj}}^2 \quad (25)$$

$$W_{cnx} = \frac{1}{2}C{v_{cnxj}}^2 \quad (26)$$

Total energy

$$W_{cx} = W_{cpx} + W_{cnx} \quad (27)$$

Ignoring power losses, the power relationship are

$$\frac{dW_{cpx}}{dt} = \left(\frac{1}{2}V_{dc} - v_x - L\frac{d_{ipx}}{dt} - Ri_{px}\right) i_{px} \quad (28)$$

$$\frac{dW_{cnx}}{dt} = \left(\frac{1}{2}V_{dc} + v_x - L\frac{d_{inx}}{dt} - Ri_{nx}\right) i_{nx} \quad (29)$$

Considering the inductor to filter the harmonic components and assuming ac side voltage and current to be sinusoidal

$$v_x = V_x \sin(\omega t) \quad (30)$$

$$i_x = I_x \sin(\omega t - \phi) \quad (31)$$

Substituting equations (28) to (31) in 27 we get

$$\frac{dW_{cx}^{\Sigma}}{dt} = -\frac{1}{2}I_xV_x\cos\varphi - R\left(\frac{I_x}{2}\right)^2 + \frac{1}{2}V_xI_x\cos(2\omega t - \varphi) - \frac{1}{2}\omega LI_x^2\sin(2\omega t - 2\varphi)$$

$$\frac{dW_{cx}^{\Sigma}}{dt} = \left[V_{dc}i_{zx} + \frac{1}{2}V_xI_x\cos\varphi - 2Ri_{zx}^2 - R\left(\frac{i_x}{2}\right)^2\right] + \left[\frac{1}{2}V_xI_x\cos(2\omega t - \varphi) + R\left(\frac{i_x}{2}\right)^2\cos(2\omega t - 2\varphi) - \frac{1}{2}\omega LI_x^2\sin(2\omega t - 2\varphi) - 2L\frac{di_{zx}}{dt}i_{zx}\right] \quad (33)$$

The Power flowing in the capacitor in each phase owns of DC elements (P_{0cx}) and low frequency ripples (P_{2cx} & P_{4cx}). Ignoring ripples, P_{0cx} is used to control the total energy stored in the capacitor

https://doi.org/10.37896/pd91.4/9146

ISSN: 0369-8963

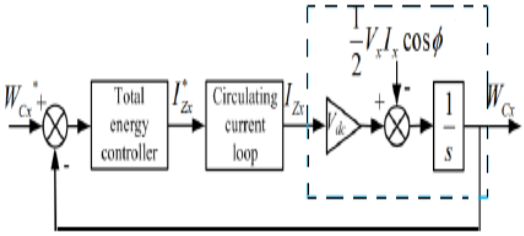

Figure 7. Total Energy Control

Modes of operation of the proposed 5-level MMC (Figure.) can be understood from the Table 1 given below considering phase 'u'

Table 1. Modes of operation in MMC

d_1	$\overline{d_1}$	d_2	$\overline{d_2}$	G_1	$\overline{G_1}$	G_2	$\overline{G_2}$	Output voltage
✓		✓			✓	✓		2Vdc
✓			✓		✓	✓		Vdc
	✓		✓					0
✓			✓	✓			✓	-Vdc
✓		✓		✓			✓	-2Vdc

Modified Instantaneous PQ theory:

H. Akagi, Kawakawa and Nabar in 1984 introduced the active and reactive power theory called the PQ theory. Since then, many contributions were given as modification to this theory. This theory can be applied for a steady state or transient state 3Φ system with or without the neutral wire. The success of the PQ theory depends on the methodology used for the decomposition of the P and Q signals into their constant and oscillating part. In the proposed modified PQ method, harmonic elimination is carried out for attaining sinusoidal output. The sinusoidal source voltage is then used for calculating the active and reactive power. The block diagram representing this entire process is significantly illustrated in the subsequent figure.

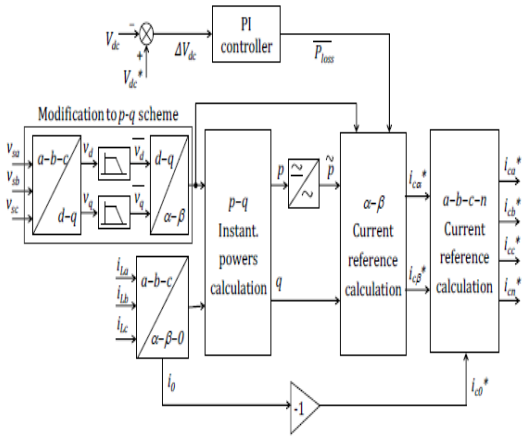

Figure 8. Block diagram of modified P-Q Theory

The a-b-c coordinates of source voltages in 3 phases (V_{sa},V_{sb},V_{sc}) get converted into to α-β, which is expressed as,

$$\begin{bmatrix} Vd \\ Vq \end{bmatrix} = \sqrt{\frac{2}{3}} \begin{bmatrix} sin\omega t & cos\omega t \\ -cos\omega t & -sin\omega t \end{bmatrix} \begin{bmatrix} 1 & \frac{-1}{2} & \frac{-1}{2} \\ 0 & \frac{\sqrt{3}}{2} & \frac{\sqrt{3}}{2} \end{bmatrix} \begin{bmatrix} v_{sa} \\ v_{sb} \\ v_{sc} \end{bmatrix} \quad (33)$$

$$\begin{bmatrix} V_\alpha \\ V_\beta \end{bmatrix} = \begin{bmatrix} cos\omega t & sin\omega t \\ -sin\omega t & cos\omega t \end{bmatrix} \begin{bmatrix} \overline{V_\alpha} \\ \overline{V_\beta} \end{bmatrix} \quad (34)$$

The load currents in all the 3 phases (i_{La}, i_{Lb}, i_{Lc}) are recognized and the coordinates are converted from a-b-c to α-β- 0.

$$\begin{bmatrix} i_0 \\ i_\alpha \\ i_\beta \end{bmatrix} = \sqrt{\frac{2}{3}} \begin{bmatrix} \frac{1}{\sqrt{2}} & \frac{1}{\sqrt{2}} & \frac{1}{\sqrt{2}} \\ 1 & -\frac{1}{2} & -\frac{1}{2} \\ 0 & \frac{\sqrt{3}}{2} & -\frac{\sqrt{3}}{2} \end{bmatrix} \begin{bmatrix} i_{la} \\ i_{lb} \\ i_{lc} \end{bmatrix} \quad (35)$$

The active and reactive power values are computed by multiplying the instantaneous α, β components of currents and voltages

$$\begin{bmatrix} p \\ q \end{bmatrix} = \sqrt{\frac{2}{3}} \begin{bmatrix} V_\alpha & V_\beta \\ -V_\beta & V_\alpha \end{bmatrix} \begin{bmatrix} i_\alpha \\ i_\beta \end{bmatrix} \quad (36)$$

$$\begin{bmatrix} i_{c\alpha}{}^* \\ i_{c\beta}{}^* \end{bmatrix} = \frac{1}{\sqrt{V_\alpha{}^2 + V_\beta{}^2}} \begin{bmatrix} V_\alpha & V_\beta \\ -V_\beta & V_\alpha \end{bmatrix} \begin{bmatrix} -\tilde{p} + \Delta\bar{p} \\ q \end{bmatrix} \quad (37)$$

$$\Delta\bar{P} = \overline{P_0} + \overline{P_{loss}} \quad (38)$$

Here, $\overline{P_0}$ signifies the required power of balancing the power inside the converter whereas $\overline{P_{loss}}$ signifies the average loss inside converter, which is obtained as,

$$\overline{P_{loss}} = k_p \Delta V_{dc} + K_i \int \Delta V_{dc} dt \quad (39)$$

Where k_p and K_i represent proportional and integral gains of PI controller. Finally, Reference filter currents $i_{ca}{}^*$, $i_{cb}{}^*$ and $i_{cc}{}^*$ in the three wires of the MMC can be obtained by following equation

https://doi.org/10.37896/pd91.4/9146

ISSN: 0369-8963

$$\begin{bmatrix} i_{ca}{}^* \\ i_{cb}{}^* \\ i_{cc}{}^* \end{bmatrix} = \sqrt{\frac{2}{3}} \begin{bmatrix} \frac{1}{\sqrt{2}} & 1 & 0 \\ \frac{1}{\sqrt{2}} & -\frac{1}{2} & \frac{\sqrt{3}}{2} \\ \frac{1}{\sqrt{2}} & -\frac{1}{2} & -\frac{\sqrt{3}}{2} \end{bmatrix} \begin{bmatrix} i_{c0}{}^* \\ i_{c\alpha}{}^* \\ i_{c\beta}{}^* \end{bmatrix} \quad (40)$$

$$i_{cn}{}^* = i_{ca}{}^* + i_{cb}{}^* + i_{cc}{}^* \quad (41)$$

Adaptive Radial Basis Function Neural Network

This paper proposes a new combination of RBFNN and modified PQ theory to control the MMC-DSTATCOM and generate the compensation reference current. Radial basis function refers to designing a curve fitting issue in large dimensional space. The RBFNN has three layers like input layer hidden layer and output layer. When a hidden unit is expanded in the hidden space, it provides arbitrary basic functions for the input pattern. A non-linear transformation takes place from input to the hidden layer whereas a linear transformation occurs among the hidden and the output layer. This neural network works on the weights and the centers to bring the optimized results. Centers are regarded as the link between input and hidden layer whereas weights are regarded as the link between hidden and output layers. RBFNN attains an optimal result depending on the positions of centers. Locating the centre is the most crucial part of the design. By clustering and averaging the centers found by multiple repetitions, the location can be approximated as closely as possible. During RBFNN learning, the unit centers are placed in locations where data is present in the input space. An increase in input vector dimension also increases the number of units, which in turn results in much faster training than the other traditional approaches. Regardless of the dimensionality of the space, it is more likely that complex pattern classification problems can be separated in the high dimensional space than in the low dimensional space, which is the basis of the learning algorithm. In the existing BPNN and RBFNN techniques, the parameters obtained after the training process are not modified once it has been completed, which can lead to degradation in performance when the training process is noisy. This paper presents a novel Adaptive RBFNN which allows the change in weights of RBFNN even after the completion of training process. It is assumed that the noise in system does not affect the input space and so there is no need to change the RBFNN centre values. The training algorithm of the proposed RBFNN has two stages. K means clustering algorithm is used in stage one to find the location of the hidden neurons' radial basis functions whereas the linear matrix inversion algorithm is employed to determine the weights between the hidden and the output layers in second stage.

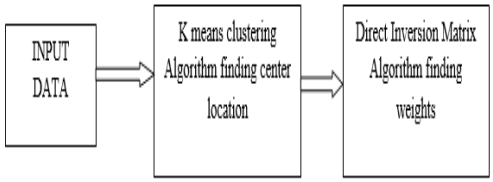

Figure 9. Flow chart of adaptive RBFNN

In order to find the center and radius of the units, the input vector is clustered. Radii is determined with 'K' nearest heuristic. In closed form, the weights are calculated based on the desired output with the center and radii fixed.

$W=A^{-1}\phi D$

Here, the desired outcome is specified as.

$$D = \begin{bmatrix} d(x1) \\ d(x2) \\ \vdots \\ d(xj) \\ \vdots \\ d(xl) \end{bmatrix} \quad (42)$$

Φ is the matrix with each element $\phi_i(xj)$ which signifies output of the i^{th} hidden neuron for the j^{th} training data sample (xj).

$$\Phi = \begin{bmatrix} \phi_1(x1) & \phi_2(x1) & \dots & \phi_k(x1) \\ \phi_1(x2) & \phi_2(x2) & \dots & \phi_k(x2) \\ \vdots & \vdots & & \vdots \\ \phi_1(xl) & \phi_2(xl) & \dots & \phi_k(xl) \end{bmatrix} \quad (43)$$

A^{-1} is the variance matrix

$A^{-1}= [\Phi^T \Phi]^{-1}$

When the summation of the output is equal to the reference signal R(k) then error is equivalent to zero and there is no need to update the weight.

$E(k) = R(K) - \{Y_1(k) + Y_2(k) + \dots\dots + Y_m(k)\}$ (44)

E(k) is used in weight updation

$W_{1new}= W_{1old} + \eta_1 \Phi(k)E(k)$ (45)

$W_{m\,new}= W_{m\,old} + \eta_m \Phi(k)E(k)$ (46)

Where η is the regulation factor

In this work, a modified instantaneous PQ theory is used which converts the current variables in the a,b,c domain to α, β domain and then the active and reactive power and components are found as

$P = \bar{P} + \tilde{P}$ (47)

$q = \bar{q} + \tilde{q}$ (48)

Here, a constant component of active power comes from the basic component is specified as $\bar{P}$ whereas a fluctuating component comes from the harmonic

 https://doi.org/10.37896/pd91.4/9146

ISSN: 0369-8963

component is specified as $\tilde{P}$. Similar process is repeated for the reactive power components $\bar{q}$ and $\tilde{q}$ .Two strategies can be used for extraction of harmonic components. In constant power strategy, the oscillating part of P, P_{loss} and q are extracted given by P_{ref} and q_{ref}

$$P_{ref} = \tilde{P} + P_{loss} \quad (49)$$

$$q_{ref} = \bar{q} + \tilde{q} \quad (50)$$

In the sinusoidal current strategy, the oscillating part of P and q and P_{loss} are extracted.

$$P_{ref} = \tilde{P} + P_{loss} \quad (51)$$

$$q_{ref} = \tilde{q} \quad (52)$$

In real world the $\tilde{q}$ is compensated by conventional power factor correction capacitor or condenser. The proposed RBFNN methodology has three stages.

(i) Building Delay Buffer

At a constant rate, the active power (P) is tested and send through the First In First out (FIFO) buffer. There will be 'N' data samples in the FIFO buffer at any time. The one sample is specified as,

$$X=[x_1 \quad x_2 \quad \dots \quad x_l] = \begin{bmatrix} P_{11} & P_{12} & \dots & P_{1l} \\ P_{21} & P_{22} & \dots & P_{2l} \\ \vdots & \vdots & \cdot & \vdots \\ P_{N1} & P_{N2} & \dots & P_{Nl} \end{bmatrix} \quad (53)$$

(ii) Finding the Desired output:

FFT is employed for each x_j for determining the constant DC part of the active power. The constant part obtained from the FFT is the desired output.

$$FFT\{x_j\} = d_i^{DC} \quad (54)$$

(iii) Training data Generation

The input 3ϕ currents and the corresponding output currents are generated through MATLAB. In the beginning, the input currents are set to zero and then increased in steps. The training process takes over thousand samples and arranges them in a vector of three rows. The size of the output vector depends on the number of output. In addition, it is recommended to have the same number of columns in both the input and output vectors. Both ideal and distorted source voltage conditions are used in the training data.

The extraction of total harmonic and reactive fundamental current from the load current I_l can be expressed as

$$I_L = A_1 \sin(\omega t + \theta_1) + \sum_{n=1}^{\infty} A_n \sin(\omega_n t + \theta_n) \quad (55)$$

$$I_L = A_1 \cos\theta_1 \sin\omega t + A_1 \sin\theta_1 \cos\omega t + \sum_{n=1}^{\infty} A_n \sin(\omega_n t + \theta_n) \quad (56)$$

Where,

$A1\cos\theta_1 \sin\omega t$ is the active fundamental current

$A_1 \sin\theta_1 \cos\omega t$ is the reactive fundamental current

$\sum_{n=1}^{\infty} A_n \sin(\omega_n t + \theta_n)$ is the total harmonics current

The Architecture of Adaptive RBFNN algorithm for the estimation of fundamental component is shown below

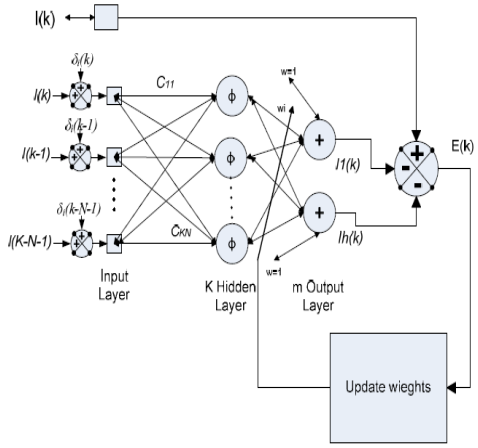

Figure 10. Structure of adaptive RBFNN

When there is no noises $\delta(k)$ in the input, the sum of RBFNN outputs is equivalent to R(k). Here E(k) = 0 and therefore there is no variations in the weight even during the noises.

$$Y_j(k) = Y_{oj}(k) + \delta_j(k) \quad (57)$$

Where, the j^{th} output node without noise is specified as $Y_{oj}(k)$ and added noise error at j^{th} node is specified as $\delta_j(k)$.

Here, $E(k) \neq 0$ and the weights are updated through least mean square algorithm. The Weights are updated until E(k) = 0

Result and Discussion

The present study intends to examine the performance efficiency of grid-tied PV system using Adaptive RBFNN based 5L MMC and the entire system is validated through MATLAB simulink for evaluating the performance metrics of the overall methodology. For validating the proposed methodology, the obtained simulink outputs are evidently illustrated in the subsequent section and the parameter specifications are clearly listed out in Table 1 in an efficient manner.

 https://doi.org/10.37896/pd91.4/9146

ISSN: 0369-8963

Table 1. Parameter Specifications

Parameters	**Values**
Solar Panel	
Short circuit current	$2.1A$
Number of solar cells connected in series	36
Number of cells in a module	9
Configuration of cells	$9\ solar\ cells * 4$
Open circuit voltage	$23.4V$
Number of modules in a panel	4
Number of panels in an array	2
5L MMC	
Number of sub-modules in each arm	2
Arm inductor	$1.50mH$
Sub-module capacitor	$0.50mF$
Arm equivalent resistance	10Ω
Load	$100\Omega, 0.1H$
Power frequency	$50Hz$
Carrier frequency	$1550Hz$

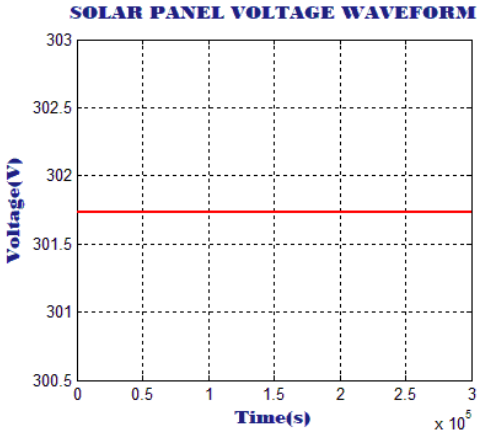

Figure 12. Output voltage of PV

The waveform representing the PV output voltage is significantly illustrated in Figure 12, which highlights that the PV delivers the output voltage of 301.7V but the attained voltage is insufficient to compensate the grid voltage and so it is given to the 5L MMC as input for maximizing the PV voltage in a wider range.

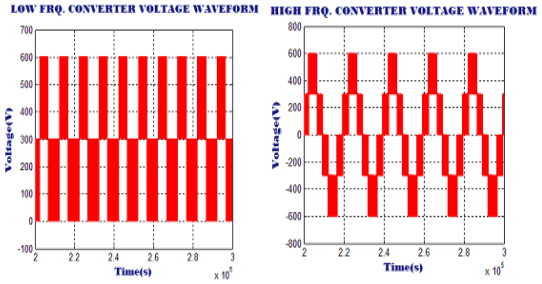

Figure 13. Waveforms of (a) Low and (High) Frequency Converter Voltage

The significance of MMC in improving the output voltage of PV is extremely high as it delivers optimal output with high efficiency both in low and high frequencies, which is evidently highlighted through the waveforms in Figure 13 in an efficient manner. As illustrated in the figure, the 5L MMC maximizes the PV output into 600V, which in turn aids in compensating the grid voltage in an optimal manner and so it is proved that the MMC delivers optimal output.

https://doi.org/10.37896/pd91.4/9146

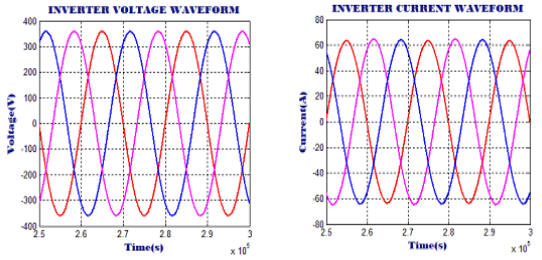

(a) (b)

Figure 14. Waveforms of (a) Inverter Voltage and (b) Current

The waveforms indicating the current and voltage of inverter are evidently illustrated in Figure 14, which displays that the inverter current is obtained as 60A whereas the inverter voltage ranges between +350V to -350V. It is thus validated that the inverter outputs are highly optimal and therefore the grid receives possibly optimal voltage, which in turn involves in accomplishing the grid voltage compensation in an efficient manner.

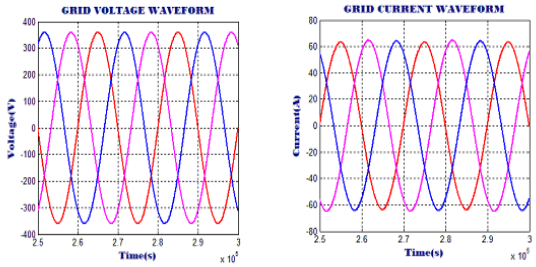

(a) (b)

Figure 15. Waveforms of (a) Grid Voltage and (b) Current

The current and voltage waveforms are clearly portrayed in Figure 15, which validates that the sinusoidal current and voltage are attained in an optimal manner. As the waveforms are sinusoidal, it is proved that the requirement of grid gets compensated in an optimal manner and hence it is summed up that the introduced 5L MMC performs well in delivering enhanced output with optimal efficiency.

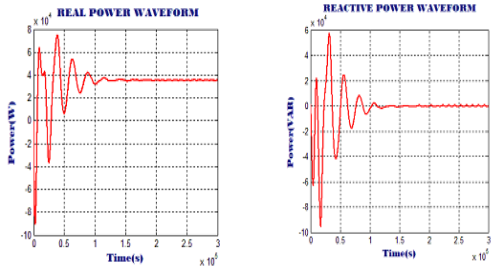

(a) (b)

Figure 16. Waveforms of (a) Real and (b) Reactive Power

The areal and reactive power waveforms are significantly highlighted in Figure 16, which shows certain oscillations in the initial stage but those fluctuations are remarkably eliminated and the constant output is attained after certain period with the assistance of 5L MMC in an efficient manner. In addition, it is observed from the waveform that the compensation is attained after the period of $4 \times 10^{-4}\ s$.

Table 2. THD Comparison

Methodologies	THD (%)
MMC with ADALINE	3.8
MMC with MLP	3.7
MMC with RBFNN	3.3
MMC with Adaptive RBFNN	2.9

The performance of introduced Adaptive RBFNN based MMC in terms of THD is analogized with other existing approaches like ADALINE, MLP and traditional ABFNN as represented in Table 2, which validates that the introduced methodology significantly outperforms other approaches with lesser THD of 2.9%.

Conclusion

The implementation of Adaptive RBFNN based 5L MMC with DSTATCOM in the Grid integrated PV system is efficiently discussed in the present study with proper analysis, which highlights that the introduced topology significantly involves in compensating the high voltage requirement of grid with maximal efficiency. The obtained DC voltage of PV is efficiently converted into AC through the implementation of 5L MMC, which is capable enough in maximizing the PV output in an wider range without necessitating much capacitors and so the complexity in implementation of this system is significantly low. In addition, the introduced theory of reference current generation known as Adaptive RBFNN involves in minimizing the harmonic in an efficient manner, which in turn results in maximizing the overall performance of the system in an optimal manner. The entire system is simulated using MATLAB and the obtained outcomes have proved the introduced methodology delivers optimal outcomes with less THD of 2.9%.

https://doi.org/10.37896/pd91.4/9146

References

1. Tuhin S Basu and Suman Maiti (Sept.-Oct. 2019) - A Hybrid Modular Multilevel Converter for Solar Power Integration. *IEEE Transactions on Industry Applications*, 55(5), 5166-5177.
2. Nirav Patel, Nitin Gupt1, and B. Chitti Babu2 (2020) - Photovoltaic system operation as DSTATCOM for power quality improvement employing active current control. *IET Gener. Transm. Distrib*., 14(17), 3518-3529.
3. Anirudh Budnar Acharya, Mattia Ricco, Dezso Sera, Remus Teoderscu and Lars E Norum (Dec. 2019) - Performance Analysis of Medium Voltage Grid Integration of PV Plant Using Modular Multilevel Converter. *IEEE Transactions on Energy Conversion*, 34(4), 1731-1740
4. Kavita Kiran Prasad, Hareesh Myneni, and Ganjikunta Siva Kumar (April 2019) - Power Quality Improvement and PV Power Injection by DSTATCOM With Variable DC Link Voltage Control from RSC-MLC. *IEEE Transactions On Sustainable Energy*, 10(2), 876-885.
5. Soumya Mishra and Pravat Kumar Ray (October 2016) - Power Quality Improvement Using Photovoltaic Fed DSTATCOM Based on JAYA Optimization. *IEEE Transactions on Sustainable Energy*, 7(4), 1672-168.
6. Marcelo A. Perez, Jose Rodriguez, Samir Kouro and Ricardo Lizana (Jan. 2015) - Circuit Topologies, Modelling, Control Schemes and Applications of Modular Multilevel Converters. *IEEE Transactions on Power Electronics*, 30(1), 4-17.
7. Jae-Jung Jung, Joon-Hee Lee, Gum Tae Son, and Yong-Ho Chung () - DC Capacitor Voltage Balancing Control for Delta-Connected Cascaded H-Bridge STATCOM Considering Unbalanced Grid and Load Conditions. IEEE Transactions on Power Electronics Volume: 33, Issue: 6, June 2018. 4726 – 4735.
8. Shengfang Fan, Kai Zhang, Jian Xiong, and Yaosuo Xue (Jan. 2015) - An Improved Control System for Modular Multilevel Converters with New Modulation Strategy and Voltage Balancing Control. *IEEE Transactions on Power Electronics*, 30(1), 358-371.
9. Hassan Mohammadi Pirouz† and Mohammad Tavakoli Bina (September 2010) - Modular Multilevel Converter Based STATCOM Topology Suitable for Medium-Voltage Unbalanced Systems. *Journal of Power Electronics*, 10(5), 572-578.
10. Krishna Kumar Gupta, Alekh Ranjan, Pallavee Bhatnagar, Lalit Kumar Sahu and Shailendra Jain (January 2016) - Multilevel Inverter Topologies With Reduced Device Count: A Review. *IEEE Transactions on Power Electronics*, 31(1), 135-151.
11. Jun Mei, Bailu Xiao, Ke Shen, Leon M. Tolbert and Jian Yong Zheng (November 2013) - Modular Multilevel Inverter with New Modulation Method and Its Application to Photovoltaic Grid-Connected Generator. *IEEE Transactions on Power Electronics*, 28(11), 5063-5073.
12. Albert Alexander and Manigandan Thathan (2015) - Modelling and analysis of modular multilevel converter for solar photovoltaic applications to improve power quality. *IET Renew. Power Gener*., 9(1), 78–88.
13. Sebastien Mari´ethoz (July 2013) - Systematic Design of High-Performance Hybrid Cascaded Multilevel Inverters With Active Voltage Balance and Minimum Switching Losses. *IEEE Transactions on Power Electronics*, 28(7), 3100-3113.
14. Arash Khoshooei, Javad S. Moghani, Ignacio Candela and Pedro Rodriguez (March/April 2018) - Control of D-STATCOM During Unbalanced Grid Faults Based on DC Voltage Oscillations and Peak Current Limitations. *IEEE Transactions on Industry Applications*, 54(2), 1680-1690.
15. Chandan Kumar and Mahesh K. Mishra (Oct. 2015) - Operation and Control of an Improved Performance Interactive DSTATCOM. *IEEE Transactions on Industrial Electronics*, 62(10), 6024-6034.
16. Hareesh Myneni and Ganjikunta Siva Kumar (2019) - Simple algorithm for current and voltage control of LCL DSTATCOM for power quality improvement. *IET Gener. Transm. Distrib*., 13(3), 423-434.
17. Tejinder Singh Saggu, Lakhwinder Singh and Balbir Gill (Spring 2017) - Harmonics Mitigation in a Steel Industry Using 11-Level Cascaded Multilevel Inverter-Based DSTATCOM. *Canadian Journal of Electrical and Computer Engineering*, 40(2), 110-115.
18. Tejinder Singh Saggu and Lakhwinder Singh (April 2016) - Comparative Analysis of Custom

 https://doi.org/10.37896/pd91.4/9146

Power Devices for Power Quality Improvement in Non-linear Loads. *2015 2nd International Conference on Recent Advances in Engineering & Computational Sciences (RAECS) IEEE Xplore* 19.

19. Eklas Hossain, Mehmet Rida Tür, Sanjeevikumar Padmanaban, Selim Ay And Imtiaj Khan (March 2018) - Analysis and Mitigation of Power Quality Issues in Distributed Generation Systems Using Custom Power Devices. *IEEE Access*, 6, 16816-16833.
20. Md. Tausif Ahmad, Narendra Kumar and Bhim Singh (2017) - Generalised neural network-based control algorithm for DSTATCOM in distribution systems. *IET Power Electron.*, 10(12), 1529-1538.
21. Gary W. Chang, Cheng-I Chen and Yu-Feng Teng (June 2010) - Radial-Basis-Function-Based Neural Network for Harmonic Detection. *IEEE Transactions on Industrial Electronics*, 57(6), 2171-2179.
22. Tah, Prakash Ch, Anup K. Panda, and Bibhu P. Panigrahi (2017) - Shunt active filter based on radial basis function neural network and pq power theory. *International Journal of Power Electronics and Drive Systems*, 8(2): 667.
23. Pratap Sekhar Puhan, Sandeep S.D, and G. Suresh Kumar - RBF Neural Network Controller In Shunt Active Power Filter. Proceedings of the Second International Conference on Computing Methodologies and Communication (ICCMC 2018) *IEEE Xplore* ISBN: 978-1-5386-3452-3.
24. M. Sivasubramanian, C. S. Boopathi, S. Vidyasagar, V. Kalyanasundaram and S. Kaliyaperumal - Performance Evaluation of Seven Level Reduced Switch ANPC Inverter in Shunt Active Power Filter with RBFNN Based Harmonic Current Generation, in *IEEE Access*, doi: 10.1109/ACCESS.2021.3064715.

 https://doi.org/10.37896/pd91.4/9146